Addressing the Stability Gap in Photoelectrochemistry: Molybdenum Disulfide Protective Catalysts for Tandem III-V Unassisted Solar Water Splitting

*Micha Ben-Naim[†1], Reuben J. Britto[†1], Chase W. Aldridge[2], Rachel Mow[2], Myles A. Steiner[3], Adam C. Nielander[1], Laurie A. King[1,4], Daniel J. Friedman[3], Todd G. Deutsch[2], James L. Young[2], Thomas F. Jaramillo[1]**

[1]Department of Chemical Engineering, Shriram Center, Stanford University, 443 Via Ortega, Stanford, California 94305, United States

[2]Chemistry and Nanoscience Center, and Materials Science Center, National Renewable Energy Laboratory, Golden, Colorado 80401, United States

[3]National Center for Photovoltaics, National Renewable Energy Laboratory, Golden, Colorado 80401, United States

[4]Faculty of Science and Engineering, Manchester Metropolitan University, Manchester M1 5GD, U.K.

[†]These authors contributed equally to this work

AUTHOR INFORMATION

Corresponding Author

*Thomas F. Jaramillo. Email: jaramillo@stanford.edu

ABSTRACT

While photoelectrochemical (PEC) solar-to-hydrogen efficiencies have greatly improved over the past few decades, advances in PEC durability have lagged behind. Corrosion of semiconductor photoabsorbers in the aqueous conditions needed for water splitting is a major challenge that limits device stability. In addition, a precious-metal catalyst is often required to efficiently promote water splitting. Herein, we demonstrate unassisted water splitting using a non-precious metal molybdenum disulfide nanomaterial catalytic protection layer paired with a GaInAsP/GaAs tandem device. This device was able to achieve stable unassisted water splitting for nearly 12 hours, while a sibling sample with a PtRu catalyst was only stable for 2 hours, highlighting the advantage of the non-precious metal catalyst. *In situ* optical imaging illustrates the progression of macroscopic degradation that causes device failure. In addition, this work compares unassisted water splitting devices across the field in terms of the efficiency and stability, illustrating the need for improved stability.

TOC GRAPHIC

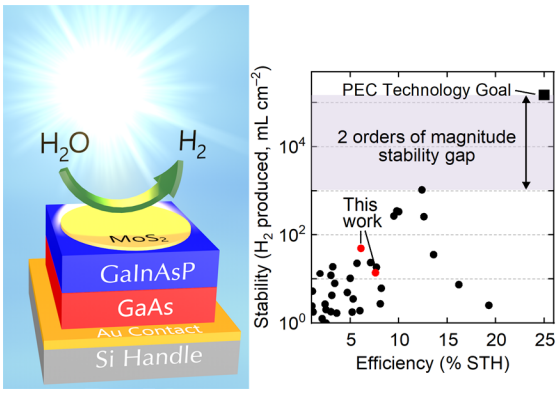

MAIN TEXT

Unassisted, solar-driven water splitting for hydrogen production via integrated solar fuels and photoelectrochemical (PEC) devices has made remarkable progress in the past several decades. Solar to hydrogen (STH) efficiencies (η_{STH}) for such systems have increased from low single digits in the 1970's to 19% in 2018.[1,2] These efficiencies nearly achieve the US Department of Energy (DOE) 2020 technical target of 20% STH efficiency and rival those of typical "off the shelf" solar cells coupled to electrolyzers.[3,4] In addition to having orders of magnitude smaller electrode areas than commercial photovoltaics (PV) and electrolyzers, these PEC devices are also still far from the 10-year lifetime goal (>17,000 h of hydrogen production with a 20% capacity factor).[3,5,6] The average commercial solar panel comes with a 25 year "lifetime guarantee", whereas the longest reported lifetime for an unassisted PEC water splitting device is only 100 hours due to the complex challenge of preventing semiconductor corrosion in aqueous environments.[4,7] While device efficiencies have been improving over the past few decades, improved stability remains a pressing research need for unassisted solar-driven water splitting that could help enable its use for sustainable hydrogen generation.

The primary strategy that has emerged to mitigate semiconductor surface corrosion is depositing thin films, such as titanium dioxide, that can act as protective barriers to prevent the electrolyte from coming into contact with the semiconductor surface.[7,8] These films have to be stable, thin enough to prevent significant light blocking, conformal, and conductive to create a stable and functional device.[9–11] Furthermore, if these films do not demonstrate intrinsic catalytic activity, an additional hydrogen and/or oxygen evolution catalyst is needed to promote efficient water splitting. Molybdenum disulfide nanomaterials have been shown to stabilize a variety of single-junction Si and III-V PEC systems, functioning as a hydrogen evolution reaction (HER) catalyst and protection layer.[9–15] Because of the promising performance in single-junction photocathodes, it is of interest to use MoS_2 with tandem semiconductor systems to improve the stability during unassisted solar water splitting.

While most III-V-based unassisted water splitting devices to date have incorporated a $Ga_{0.51}In_{0.49}P$ (hereafter $GaInP_2$) (1.8 eV) top cell, device lifetimes have been limited to <100 h.[7,16] $Ga_xIn_{1-x}As_yP_{1-y}$ (1.7 eV) has shown promise as a PV material and has been paired with a $Ga_zIn_{1-z}As$ bottom cell (1.1 eV) for efficient tandem PV systems, motivating efforts to incorporate $Ga_xIn_{1-x}As_yP_{1-y}$ into PEC systems and investigate the stability of this quaternary top cell.[16–19] The composition of $Ga_xIn_{1-x}As_yP_{1-y}$ (hereafter GaInAsP), nominally $x \sim 0.68$ and $y \sim 0.34$, gives the desired bandgap of 1.7 eV and a lattice constant matching that of GaAs.[16,18] A GaInAsP/GaAs (1.7/1.4 eV) pairing has a predicted maximum STH efficiency of ~12%,[16,19] far from the ideal combination of absorbers to achieve the highest of efficiencies, however sufficiently high to perform durability studies on active, unassisted water splitting systems, guiding the design of a

more efficient tandem PEC structure pairing GaInAsP with a more optimal bottom absorber (bandgap ~ 1.05 eV).[16,19]

In this letter, we showcase molybdenum disulfide thin films as a stabilization strategy for unassisted water splitting devices. Tandem pn-GaInAsP/pn-GaAs water splitting devices were fabricated with either a molybdenum disulfide thin film or nanoparticulate PtRu catalyst, and both demonstrated unassisted water splitting. While the two devices showed similar efficiencies, the MoS_2 device was stable >5 times longer than the PtRu device (11.8 vs 2.2 h). *In situ* optical microscopy was used to characterize failure mechanisms of the devices. We also analyze the best unassisted water splitting devices across the field in terms of their efficiencies and stabilities to quantify the stability gap and to reveal insights into how we, as a field, can close it.

Two device architectures with identical tandem III-V absorbers (pn-GaInAsP/pn-GaAs) and different catalysts/protection layers (MoS_2 or PtRu) were tested in this study (Figure 1). Detailed descriptions of device fabrication can be found in section 1 of the Supporting Information.[20] Briefly, the absorbers were fabricated by inverted epitaxy to incorporate an Au back reflector that has been shown to improve photon absorption in the bottom cell.[16] An MoS_2 coating was deposited on the MoS_2/pn-GaInAsP/pn-GaAs device (hereby known as MoS_2/III-V) by sputtering a nominal 3.6 nm Mo metal film followed by a thermal partial sulfidization (Figure 1).[9–11] This MoS_2 coating procedure is identical to that performed in a previous study on MoS_2-coated $GaInP_2$ phocathodes; X-ray photoelectron spectroscopy (XPS) demonstrated that the catalyst coating comprised a mixture of MoS_2, metallic Mo, and MoO_x.[9] In another work developing MoS_2/n^+p-Si photocathodes with a MoS_2 deposition process utilizing a slightly higher sulfidization temperature

but otherwise identical to that in this work, cross-sectional transmission electron microscopy (TEM) imaging demonstrated a thickness of ~5 nm, with MoS_2 sheets residing on top of a thin metallic Mo layer.[10] Based on these previous results, the MoS_2 layer is expected to have some sulfide, metallic, and oxide character and a thickness of ~5 nm. For the PtRu/pn-GaInAsP/pn-GaAs device (hereby known as PtRu/III-V), a flash sputtering process that has been shown to deposit metallic PtRu 2-5 nm nanoparticles[9,21] was utilized to deposit this catalyst onto a different piece of the same wafer used for the MoS_2/III-V device . The same PtRu flash sputtering was also used in coating a 16.2%-efficient tandem III-V cell, one of the highest STH efficiencies for an integrated PEC device reported to date (Figure 1),[1,16] so the PtRu/III-V sample represents a competitive comparison point for the MoS_2-protected device.

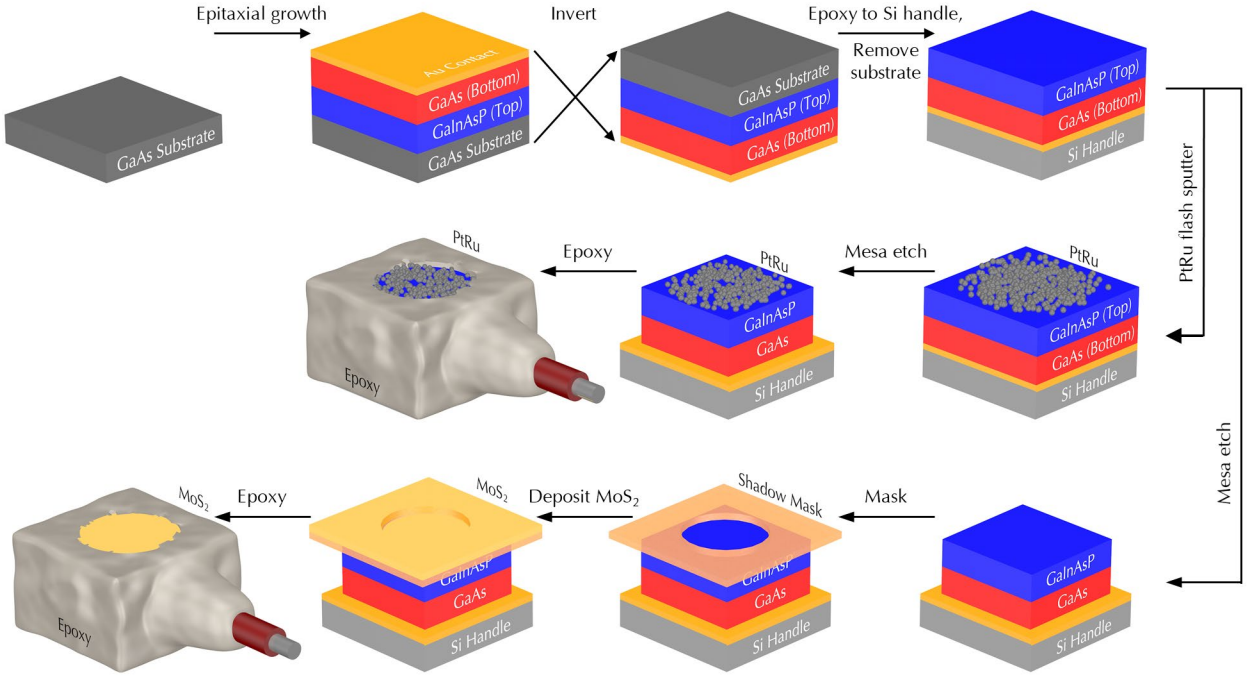

Figure 1. Fabrication scheme for the MoS_2/pn-GaInAsP/pn-GaAs (first and third rows) and PtRu/pn-GaInAsP/pn-GaAs devices (first and second rows). Both devices originated from the same growth, and the wafer was cleaved in half prior to catalyst deposition.

Following an established protocol[16,22,23] (see Experimental Methods section), the PEC performance of the MoS_2/III-V and PtRu/III-V devices was evaluated via linear sweep voltammetry (LSV) in a one-compartment cell under a quartz tungsten-halogen illumination source calibrated to 1.3 suns with a $GaInP_2$ reference diode, representing an overall illumination power of ~1.2 suns across the full spectrum.[24,25] Two-electrode LSVs were conducted with bias applied vs. the RuO_2 counter electrode (Figure 2a). Three-electrode LSVs incorporated the RuO_2 counter electrode and a $Hg/HgSO_4$ reference electrode for conversion to a reversible hydrogen electrode (RHE) scale and were measured for the two devices and a replicate of each structure (Figure S2a). For both device structures, the photoelectrode functions as a photocathode, with the MoS_2 or PtRu catalyst facilitating the HER ($2H^+ + 2e^- \rightarrow H_2$) and the RuO_2 anode counter electrode catalyzing the oxygen evolution reaction (OER) ($2H_2O \rightarrow O_2 + 4H^+ + 4e^-$). A band diagram schematic is shown in Figure S1. Scans were taken from a reverse bias (–0.5 V vs RuO_2) to more positive bias to determine the onset voltage and light-limited photocurrent density. The first ~ 100 mV of both the two-electrode and three-electrode LSVs was measured with the light blocked to observe the dark current. Both devices had minimal dark current at the most negative applied bias, indicating that the observed current under illumination is due to light absorption (Figure 2a). The voltammogram was halted when the current density reached –0.5 mA cm^{-2} to prevent any surface oxidation associated with passing anodic current (Figure 2a). The LSV was immediately followed by a chronoamperometry (CA) measurement conducted at short circuit (E = 0 V vs RuO_2) (Figure 2b).

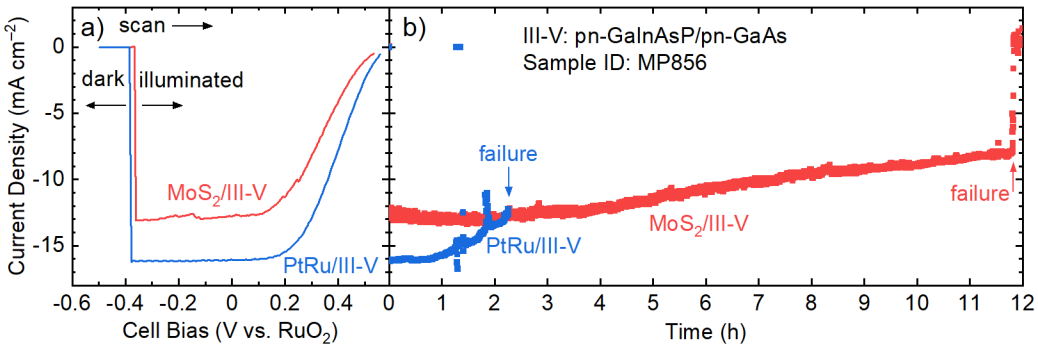

Figure 2. Electrochemical characterization of the MoS_2/III-V and PtRu/III-V unassisted water splitting devices in 0.5 M sulfuric acid. a) Two-electrode LSV collected prior to stability testing. The scan was measured from negative to positive applied bias with a scan rate of 20 mV s^{-1}, with the first 100 mV measured with light blocked, and the remainder measured under illumination. b) CA measurement taken at short circuit (E = 0 V vs RuO_2) until device failure. Both measurements utilized a quartz-tungsten halogen lamp with ~2.6-sun-equivalent illumination.

The MoS_2/III-V device demonstrated an onset voltage of 0.50 V vs RuO_2 (Figure 2a), while the PtRu/III-V device had an onset voltage of 0.54 V vs RuO_2, where the onset voltage is defined here as the applied voltage required to reach a current density of –1 mA cm^{-2}. The three-electrode measurements confirmed that the MoS_2/III-V and PtRu/III-V devices produced high photovoltages (Figure S2a). Replicate samples exhibited onset potentials within 0.07-0.08 V of the sibling samples tested in Figure 2, and the average onset potential for the MoS_2/III-V and PtRu/III-V devices in the three-electrode measurements were 1.92 and 1.96 V vs. RHE, respectively, a consistent trend to that observed in the two-electrode measurements. The positive onset potential and corresponding high photovoltage are expected for the PtRu/III-V device given that it matches the paradigm common to the highest efficiency PEC devices: high-quality III-V semiconductors coupled to a Pt-based catalyst.[1,8] The similar onset voltage of the MoS_2/III-V and PtRu/III-V

devices may be surprising as the nanoparticulate PtRu is a better HER catalyst than planar MoS_2, with the PtRu catalyst having been shown to require ~0.25 V less overpotential to achieve a current density of –10 mA cm^{-2} than the MoS_2 catalyst.[9,11,26,27] However, the conformality of MoS_2 has previously been shown to improve charge carrier extraction at the surface compared to a III-V-electrolyte interface, leading to similar onset voltages between the two devices.[11,28]

Under the tungsten halogen lamp illumination, the MoS_2/III-V device achieved a light-limited current density of –12.8 mA cm^{-2}, while the PtRu/III-V device achieved –16.0 mA cm^{-2} (Figure 2a). The lower photocurrent density observed for the MoS_2/III-V system compared to that of the PtRu/III-V is attributed to the partially sulfidized MoS_2 layer which contains some Mo content that has been shown to cause parasitic absorption.[9–11] The two systems yielded greater photocurrent densities than what might be anticipated for this particular tandem III-V system under an overall illumination of ~1.2 suns (see earlier discussion regarding the bandgap values). However, it is important to note that a tungsten lamp spectrum deviates significantly from the true solar spectrum across the absorbable photon range. Thus, great care must be taken in calculating STH efficiency values (Figure S3).[25,29] Due to these spectral differences, a calculation of η_{STH} based on measurements using such a light source can never be fully representative of that under true solar irradiance; however, there are strategies to improve the accuracy. For this particular tandem device, it is the large bandgap of the bottom junction that limits device photocurrent under AM1.5G illumination, and thus it is the photon flux to the bottom junction that determines device performance. In this region of the spectrum, the photon flux of our tungsten lamp was measured at ~2.6 × that of the AM1.5G spectrum; hence this value was used to estimate the incident power of solar irradiance that would be needed to yield the same measured current densities, i.e. the

equivalent number (n) of suns (Table S2). This conservative estimate yields η_{STH} values of roughly 6.1 and 7.6% for the MoS_2/III-V and PtRu/III-V devices, respectively. Full details of the tungsten lamp spectrum and η_{STH} estimation can be found in sections 3 and 4 of the Supporting Information.[30–32] While the light source used herein was selected for the superior bulb lifetime and output stability, which are desirable for durability measurements that are key to this study, improved benchmarking protocols for PEC efficiency such as using incident-photon-to-current efficiency (IPCE) measurements to calculate spectral correction factors and employing a light source that more accurately matches the solar spectrum should be used for determination of η_{STH} and comparison with other reports.[16,25]

Stability of the devices was measured via chronoamperometry with no applied bias in a two-electrode configuration under tungsten lamp illumination with the same intensity as used in the LSV measurements (Figure 2b). We expect similar charge carrier dynamics at the electrolyte-GaInAsP interface whether under the tungsten lamp illumination used here or under solar illuminationbecause either way, the bottom cell is expected to be current-limiting (Figure S4), and thus the top cell potential will be pinned at open circuit voltage. Hence, stability measurements under tungsten lamp illumination are representative of behavior under solar illumination. *In situ* optical microscope time-lapse movies were collected during the stability test to monitor macroscopic degradation (Movies S1,2). The MoS_2/III-V device maintained its initial light-limited current density for ~4 h without a loss in photocurrent, after which time the photocurrent density started slowly decreasing until a sudden drop to nearly 0 mA cm^{-2} at 11.8 h (Figure 2b). This sudden decrease in current corresponds to macroscopic degradation observed optically from t = 11.6 h to 11.8 h (Figure 3, Movie S1). A ~0.8 mm circular defect appeared at 8.2 h, during the

period when the current density was slowly decreasing, although this defect did not have an immediate impact on the current density, indicating that the current decrease was due to microscopic rather than macroscopic degradation. However, this defect started to grow at 11.6 h, with the entire surface appearing to bubble and delaminate shortly after at 11.7 h, indicating more rapid material degradation concomitant with the observed current loss. This degradation continued with large-scale material deformation apparent at 11.8 h. The MoS_2/III-V replicate device lasted 4.0 h until a sudden failure, which indicates that both MoS_2/III-V devices suffered similar failure mechanisms MoS_2/III-V (Figure S2b). The PtRu/III-V device demonstrated much less durability than the MoS_2/III-V devices, maintaining its initial photocurrent density of –16 mA cm^{-2} for ~1 h followed by decreasing photocurrent until a sudden failure at 2.2 h (Figure 2b). At 1.3-1.4 h, a diagnostic repositioning of the photoelectrode was performed to determine if the decline in photocurrent was related to bubble accumulation on the surface. This repositioning caused the current to momentarily drop to 0 and can be observed in the microscope time lapse during this time (5:00 – 5:35 in Movie S2). After repositioning, the photocurrent returned to the same trajectory, indicating that the majority of the decline in photocurrent was not due to bubble accumulation but to material degradation. At 2.15 h, a defect, identified by darker contrast in the optical microscope images, started to form near the edge of the device. This defect grew quickly until the test was stopped at 2.2 h when roughly a quarter of the electrode surface had degraded. During the initial decrease in current density between 1-2 h of testing, there were no macroscopic defects visible; however, the sharper decrease in current after 2 h was likely due to the large-scale degradation. Additional experimentation using the *in situ* microscopy technique presented in this work could allow for identification of other macroscopic degradation features that impact device performance and stability.

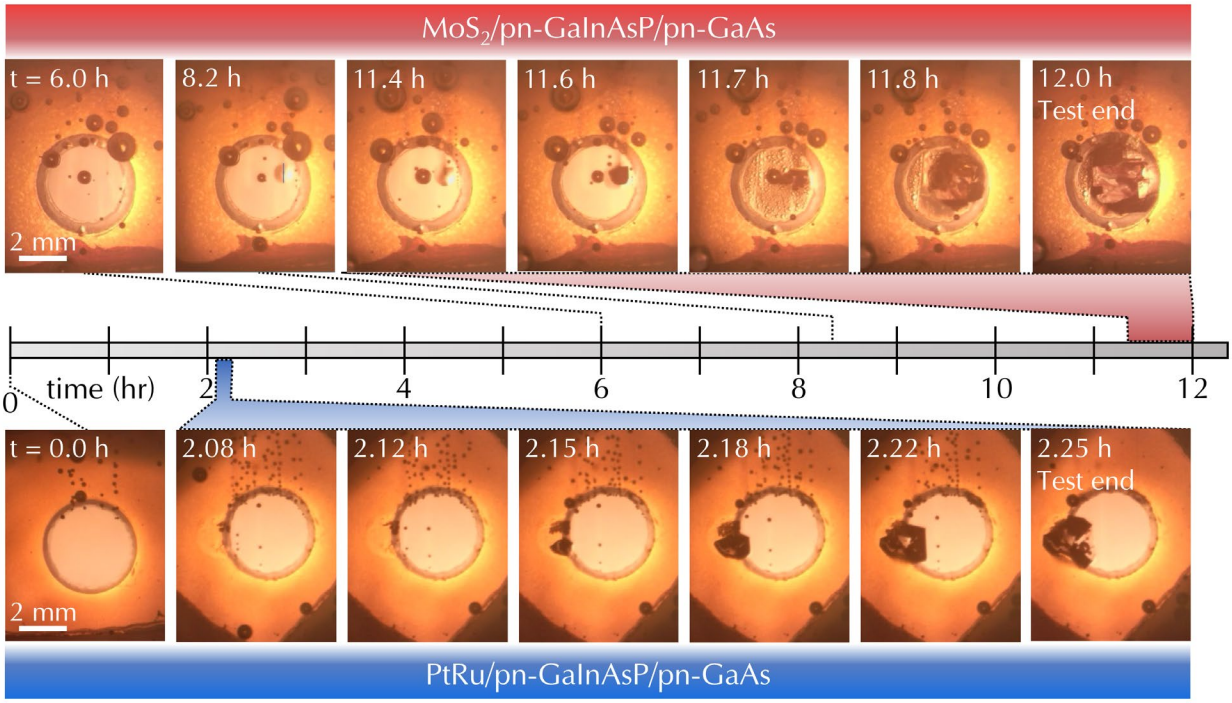

Figure 3. Optical microscope images of PEC devices during stability testing. Selected images from the time lapse for the (top row) MoS_2/III-V device and (bottom row) PtRu/III-V device. Defects are identified by darker contrast in the images. Full, high-resolution time lapse movies can be seen in the supporting information (Movies S1,S2).

The MoS_2/III-V device lasted over five times longer than the PtRu/III-V device, which is consistent with enhanced durability as observed in previous reports comparing MoS_2- and PtRu-coated $GaInP_2$ photocathodes.[9,11,12] As seen in the microscope images, both the MoS_2/III-V and PtRu/III-V devices had similar failure modes, where macroscopic degradation originated at a single point, likely a material growth or post-growth processing defect. This degraded area then rapidly grew to encompass the whole sample, leading to a sudden loss in current. The PtRu catalyst is deposited as 2-5 nm nanoparticles and therefore exposes the GaInAsP surface to the acidic

electrolyte in which III-V semiconductors are known to degrade, likely resulting in a more rapid failure mechanism.[9,11,33,34] Conversely, the conformal nature of the MoS_2 catalyst and the intrinsic stability of MoS_2 in acidic environments would protect the GaInAsP surface from corrosion, leading to a longer timescale of degradation and improved device longevity.[9–12,15,35] *Operando* spectroscopy and microscopy techniques such as *operando* X-ray absorption spectroscopy (XAS) and scanning photoelectrochemical microscopy (SPECM) could allow for identification of the chemical nature of material defects and illustrate how the chemical state and electrochemical properties of the devices evolve over the course of testing, motivating future investigations.[36–39]

These results demonstrate that a non-precious metal conformal catalyst such as MoS_2 may actually be preferred over a Pt-based precious metal catalyst as the substantial stability improvements and lower cost may outweigh the minor loss in photoelectrode activity. Although the inverted III-V epitaxial growth process used here involves etching the expensive GaAs wafer substrate, strategies to reuse the GaAs substrate including epitaxial lift-off[40] or spalling[41], combined with the use of low-cost hydride vapor-phase epitaxy[42] to grow the device structure could drastically reduce the cost of the semiconductor growth.[43] Future work will focus on improving the light-limited current density of MoS_2-protected devices through strategies such as increasing the transparency of the MoS_2 layer by optimizing the degree of sulfidization and incorporating light-trapping structures. In addition, the PtRu/GaInAsP/GaAs device explored here had a longer lifetime than a PtRu/$GaInP_2$/GaInAs sample fabricated by inverted metamorphic epitaxy that lost ~25% of its current density over 1.2 h.[16] This promising stability for the device with a GaInAsP top cell indicates that this material could be suited for durable PEC systems and

provides motivation for pairing GaInAsP with a lower bandgap (~1.05 eV) bottom cell than GaAs to improve the efficiency.[16,19]

To assess the results presented in this work and quantify the progress made by the field of photoelectrochemistry, we compare reports of unassisted PEC water splitting systems. Semiconductor corrosion in electrolyte is a major barrier to PEC stability, so integrated PEC devices are subject to different stability constraints and design considerations than PV-electrolysis systems despite the similar physics governing device operation.[44] For the purposes of this study, solar water splitting devices with a photoelectrode are considered, where the photoelectrode must contain at least one semiconductor absorber tightly integrated with a catalyst (i.e. not easily mechanically separated).

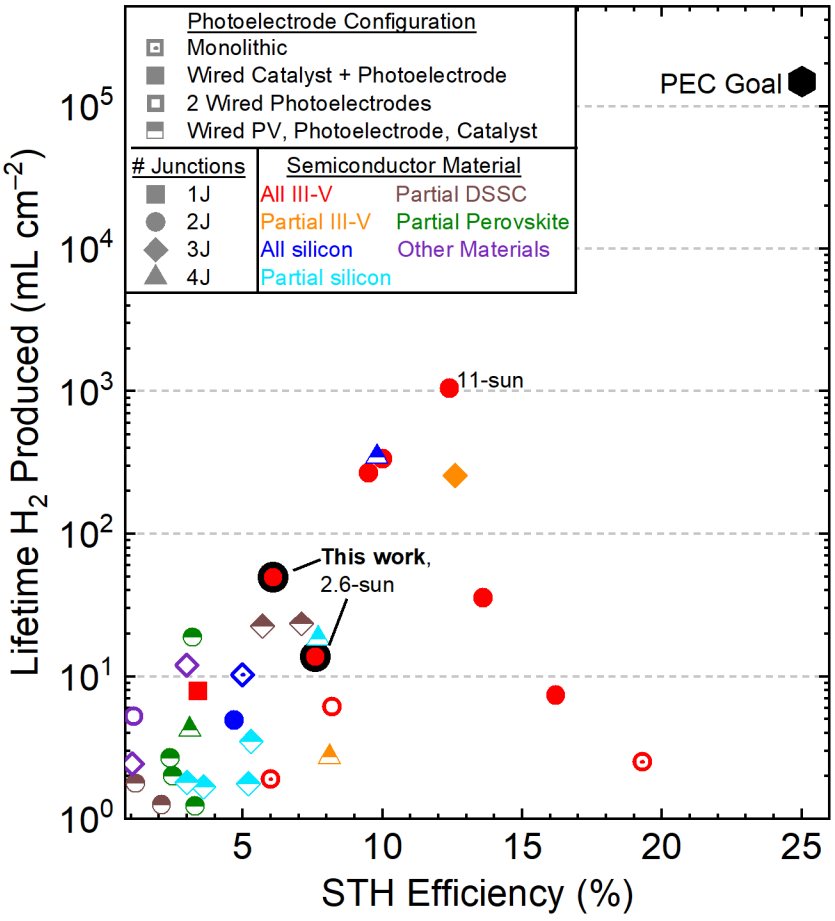

Figure 4. Comparison of the solar to hydrogen efficiency and lifetime H_2 produced for high performing (>1% STH and >1 mL cm^{-2} H_2) unassisted water splitting devices with at least one photoelectrode comprised of a catalyst integrated with one or more semiconductors. The "PEC Goal" point in the upper right were calculated assuming a 20% capacity factor over a 10 year lifetime. The tabulated data from this figure can be found in Tables 1 and 2.[2,16,52–61,21,62–71,45–51]

These solar-driven water splitting devices have several device architectures: 1) A monolithic device integrating semiconductor(s), an HER catalyst, and an OER catalyst without wires. 2) One photoelectrode integrating semiconductor(s) and either an HER catalyst or an OER catalyst, which is wired to a counter electrode. 3) Two photoelectrodes, each of which integrates a semiconductor

and one catalyst, which are wired together, and 4) A photoelectrode, which is wired to a separate solid-state PV and a separate catalyst. For all systems, standard temperature and pressure (STP) was used to calculate a volume of hydrogen produced, and a 100% faradaic efficiency to hydrogen was assumed. Figure 4 encompasses only unassisted solar water splitting devices that have produced >1 mL cm^{-2} of hydrogen gas during a durability study and have an STH >1%. Details on devices with architectures 1-3 are tabulated in Table 1, while those for devices with a wired photoelectrode, catalyst, and PV(s) are tabulated in Table 2. A comparison of unassisted solar water splitting devices that have an initial STH efficiency >1% that produced <1 mL cm^{-2} H_2 are found in Figure S5 and tabulated in Tables S3 and S4.[72-91]

The "PEC Goal" point in the upper right of Figure 4 represents the DOE's long-term PEC technology goal of 25% η_{STH} and a 10-year lifetime and was calculated assuming a 20% capacity factor (or ~5 h of 1-sun illumination per day).[5,6] Notably, the device that has produced the most hydrogen to date[45] is two orders of magnitude behind the PEC field's ultimate goal, illustrating a stability gap (Figure 4). Conversely, device efficiencies have been improving in recent years, with a series of reports exceeding 13%,[21] 16%,[16] and 19% STH efficiency.[2] Although improving efficiency has been and will continue to be an important priority, improving stability going forward is an important challenge that should be given high priority. A successful stabilization strategy for many PEC water splitting devices is to use a thin film to protect the semiconductor surface from corrosion (Figure 4, Tables 1, 2), which has led to devices with 100 h of stability for unassisted water splitting.[7] Protective thin films could yield improved durability as single junction photocathodes with similar MoS_2 thin films to those presented in this work have demonstrated months of stability;[92] however, the stability of devices during unassisted water splitting (two-

electrode) conditions is fundamentally different than that probed by three-electrode chronoamperometry measurements.[16] The DOE target for PEC water splitting is an important goal for the field, and even though specific applications will dictate different efficiency and stability targets than the single DOE goal, all applications of PEC technology will be enhanced by improved stability.

In summary, MoS_2 nanomaterials were used as a non-precious metal catalytic protection layer to stabilize a pn-GaInAsP/pn-GaAs tandem unassisted water splitting device and catalyze hydrogen evolution efficiently. The MoS_2-protected device demonstrated nearly 12 h stability and similar activity to a PtRu-catalyzed pn-GaInAsP/pn-GaAs tandem device that only lasted 2.2 h, indicating that a non-precious metal catalyst may have advantages compared to precious metals due to the improved stability and lower cost. The quaternary GaInAsP top cell also demonstrated promising stability and could be paired with a low bandgap (~1.05 eV) semiconductor to improve device efficiency. These devices were then compared to the best unassisted water splitting devices to date in terms of their stabilities and efficiencies. This comparison revealed a two orders of magnitude "stability gap" that exists between the current state of the art and the ultimate 10-year lifetime goal.

Table 1. Tabulated data of unassisted water splitting devices consisting of photoelectrodes and/or catalysts without a separate, wired photovoltaic. Semiconductor materials are shown in black, catalysts are in red, and protecting/contact layers are in blue.

(Photo)cathode	(Photo)anode	Configuration	Initial STH (%)	Stability (h)	Average *J* (mA cm^{-2})	Charge Passed (C)	H_2 Produced (mL cm^{-2})	First Author	Year	Ref #
Pt/p-$GaInP_2$/pn-GaAs	Pt	Wired catalyst	12.4[1]	20	125	9000	1040	Khaselev	1998	45
CoPi	Ni/TiO_2/$GaInP_2$/GaAs	Wired catalyst	10.0	100	8	2900	330	Sun	2016	7
NiMo	Ni/$GaInP_2$/GaAs	Wired catalyst	9.5	80	8	2300	270	Verlage	2015	46
Pt	Pt/GaN/$GaInP_2$/GaAs/Ge	Wired catalyst	12.6	70	8.8	2200	260	Wang	2019	47
MoS_2/pn-GaInAsP/pn-GaAs	RuO_2	Wired catalyst	6.1[2]	11.8	10	430	49	Britto, Ben-Naim	2020	This work
PtRu/pn-$GaInP_2$/QW/GaAs	IrO_x	Wired catalyst	13.6	10	8.5	310	36	Steiner	2019	21
PtRu/pn-GaInAsP/pn-GaAs	RuO_2	Wired catalyst	7.6[2]	2.2	15	140	14	Britto, Ben-Naim	2020	This work
RuO_x/TiO_2/Ga_2O_3/Cu_2O	Mo:$BiVO_4$	Two wired photoelectrodes	3.0	12	2.4	100	12	Pan	2018	48
Pt/pin-Si/pin-Si/pin-Si/	RuO_2	Monolithic	5.0	5.83	4.2	89[3]	10.	Lin	1989	49
Pt/InGaN NW/Si	Pt	Wired catalyst	3.4	7	2.7	68	7.9	Wang	2019	50
PtRu/$GaInP_2$/GaInAs	RuO_2	Wired catalyst	16.2	1.3	13.6	64	7.4	Young	2017	16
Pt/p-InP	MnO/n-GaAs	Two wired photoelectrodes	8.2	1.33	11	53	6.1	Kainthla	1987	51
Pt/Mo/Ti/ZnSe-CIGS/	Pt/CoO_x /$BiVO_4$	Two wired photoelectrodes	1.1	21	0.6	45	5.3	Higashi	2017	52

NiMoZn	CoPi/ITO/a-Si/a-Si/a-Si	Wired catalyst	4.7	3	3.9	42	4.9	Reece	2011	53
Rh/TiO_2/$AlInPO_x$/AlInP/GaInP	RuO_x/GaInAs/ GaAs	Monolithic	19.3	0.5	12	22	2.5	Cheng	2018	2
Pt/ HfO_2/CdS/CZTS	$BiVO_4$	Two wired photoelectrodes	1.0	10	0.58	21	2.4	Huang	2018	54
Pt/TiO_x/GaInP/GaAs	Ni/NiO_x	Monolithic	6.0	1	4.4[3]	16[3]	1.9	Varadhan	2019	55

[1]11-sun illumination

[2]~2.6-sun illumination

[3]H_2 production was reported. Current density and charge passed are calculated from the H_2 production rate

Table 2. Tabulated data of unassisted water splitting devices consisting of at least one photoelectrode, wired photovoltaic(s), and a wired catalyst. Semiconductor/PV materials are shown in black, catalysts are in red, and protecting/contact layers are in blue.

(Photo)cathode	(Photo)anode	Photovoltaic	Initial STH (%)	Stability (h)	Average *J* ($mA\ cm^{-2}$)	Charge Passed (C)	H_2 Produced ($mL\ cm^{-2}$)	First Author	Year	Ref #
NiMo/pn^+-Si	NiMO/np^+-Si	c-Si/c-Si	9.8	105	7.9	3000	350	Fan	2019	56
Pt	(FeOOH/NiOOH)/	DSSC	7.1	10	5.6	200	23	Shi	2016	57
Pt	(FeOOH/NiOOH)/$BiVO_4$/WO_3	DSSC	5.7	12	4.5	190	23	Shi	2015	58
Pt	Mo:$BiVO_4$/Co-Ci	Perovskite	3.2	12	3.8	160	19	Kim	2015	59
Pt	(FeOOH/NiOOH)/$BiVO_4$/Fe_2O_3	c-Si/c-Si	7.7	8	5.5	160	18	Kim	2016	60
MoS_x	CoPi/$BiVO_4$	Perovskite/Perovskite/ Perovskite	3.1	4.5[1]	2.3	37	4.2	Zhang	2020	61
Ni/CoP	CoO_x/$BiVO_4$	c-Si/c-Si	5.3	2	4.2	30	3.5	Kim	2018	62
Pt	CoPi/ $BiVO_4$/WO_3	GaAs/InGaAsP	8.1	1	6.5	23	2.7	Kosar	2016	63
Pt	CoPi/Fe_2O_3	Perovskite	2.4	8	0.8	23	2.7	Gurudayal	2015	64
RuO_2/TiO_2/AZO/Cu_2O	IrO_2	Perovskite	2.5	2.67	1.8	17	2.0	Dias	2015	65
Pt	WO_3	a-Si/a-Si	3	1.67	2.7	16	1.8	Gaillard	2010	66
Pt	Fe_2O_3	DSSC	1.2	8.5	0.5	15	1.8	Brillet	2012	67
Pt	CoPi/n-$BiVO_4$	a-Si-H:/a-Si:H	5.2	1	4.2	15	1.8	Han	2014	68
Pt	CoPi/n-$BiVO_4$	pin-Si/pin-Si	3.6	1	4	14	1.7	Abdi	2013	69
Pt	CdSe/CdS/TiO_2 NT	DSSC	2.1	2	1.5	11	1.3	Shin	2015	70

Pt	Ni/SnO_2/In_2S_3/$CdIn_2S_4$	Perovskite	3.3	1.5	1.9	11	1.2	Meng	2020	71

[1]6 hours of cycled testing (0.75 h illuminated, 0.25 h dark)

ASSOCIATED CONTENT

Supporting Information. The following files are available free of charge.

Experimental methods and materials, additional electrochemical measurements, lamp spectrum, limiting junction calculations, and an expanded comparison plot showing unassisted water splitting devices with >1% STH efficiency and any stability reported (PDF)

In situ stability time lapse movies (mp4)

AUTHOR INFORMATION

Corresponding Author

*E-mail: jaramillo@stanford.edu. Phone: (650) 498 6879

Notes

The authors declare no competing financial interests.

ACKNOWLEDGMENT

This paper presents results from a United States Department of Energy Office of Energy Efficiency and Renewable Energy (EERE) , Fuel Cell Technologies Office project (award number DE-FOA-0001647) competitively-selected under the solicitation "Topic 2A: Durable, High-Performance Materials and Interfaces for Advanced Water Splitting". The authors gratefully acknowledge research support from the HydroGEN Advanced Water Splitting Materials Consortium, established as part of the Energy Materials Network under the U.S. Department of Energy, Office of Energy Efficiency and Renewable Energy, Fuel Cell Technologies Office, under Contract Number DE-AC36-8GO28308 to the National Renewable Energy Laboratory (NREL).

Work was performed in part at the Stanford Nano Shared Facilities (SNSF) and the nano@Stanford labs (SNF), which are supported by the National Science Foundation as part of the National Nanotechnology Coordinated Infrastructure under award ECCS-1542152. RJB acknowledges support from the National Science Foundation Graduate Research Fellowship Program. The views expressed in the article do not necessarily represent the views of the DOE or the U.S. Government. The U.S. Government retains and the publisher, by accepting the article for publication, acknowledges that the U.S. Government retains a nonexclusive, paid-up, irrevocable, worldwide license to publish or reproduce the published form of this work, or allow others to do so, for U.S. Government purposes.

REFERENCES

(1) Ager, J. W.; Shaner, M. R.; Walczak, K. A.; Sharp, I. D.; Ardo, S. Experimental Demonstrations of Spontaneous, Solar-Driven Photoelectrochemical Water Splitting. *Energy Environ. Sci.* **2015**, *8*, 2811–2824, DOI: 10.1039/c5ee00457h.

(2) Cheng, W.-H.; Richter, M. H.; May, M. M.; Ohlmann, J.; Lackner, D.; Dimroth, F.; Hannappel, T.; Atwater, H. A.; Lewerenz, H.-J. Monolithic Photoelectrochemical Device for Direct Water Splitting with 19% Efficiency. *ACS Energy Lett.* **2018**, *3*, 1795–1800, DOI: 10.1021/acsenergylett.8b00920.

(3) United States Department of Energy. *Fuel Cell Technologies Office Multi-Year Research, Development, and Demonstration Plan, 2015*; 2015.

(4) SunPower Corporation. *SunPower E20-327-D-AC Datasheet*; 2018.

(5) Sathre, R.; Greenblatt, J. B.; Walczak, K.; Sharp, I. D.; Stevens, J. C.; Ager, J. W.; Houle, F. A. Opportunities to Improve the Net Energy Performance of Photoelectrochemical Water-Splitting Technology. *Energy Environ. Sci.* **2016**, *9*, 803–819, DOI: 10.1039/c5ee03040d.

(6) Shaner, M. R.; Atwater, H. A.; Lewis, N. S.; McFarland, E. W. A Comparative Technoeconomic Analysis of Renewable Hydrogen Production Using Solar Energy. *Energy Environ. Sci.* **2016**, *9*, 2354–2371, DOI: 10.1039/c5ee02573g.

(7) Sun, K.; Liu, R.; Chen, Y.; Verlage, E.; Lewis, N. S.; Xiang, C. A Stabilized, Intrinsically Safe, 10% Efficient, Solar-Driven Water-Splitting Cell Incorporating Earth-Abundant Electrocatalysts with Steady-State PH Gradients and Product Separation Enabled by a Bipolar Membrane. *Adv. Energy Mater.* **2016**, *6*, 1600379, DOI: 10.1002/aenm.201600379.

(8) Hu, S.; Lewis, N. S.; Ager, J. W.; Yang, J.; McKone, J. R.; Strandwitz, N. C. Thin-Film Materials for the Protection of Semiconducting Photoelectrodes in Solar-Fuel Generators. *J. Phys. Chem. C* **2015**, *119*, 24201–24228, DOI: 10.1021/acs.jpcc.5b05976.

(9) Britto, R. J.; Young, J. L.; Yang, Y.; Steiner, M. A.; LaFehr, D. T.; Friedman, D. J.; Beard, M. C.; Deutsch, T. G.; Jaramillo, T. F. Interfacial Engineering of Gallium Indium Phosphide Photoelectrodes for Hydrogen Evolution with Precious Metal and Non-Precious Metal Based Catalysts. *J. Mater. Chem. A* **2019**, *7*, 16821–16832, DOI: 10.1039/C9TA05247J.

(10) Benck, J. D.; Lee, S. C.; Fong, K. D.; Kibsgaard, J.; Sinclair, R.; Jaramillo, T. F. Designing Active and Stable Silicon Photocathodes for Solar Hydrogen Production Using Molybdenum Sulfide Nanomaterials. *Adv. Energy Mater.* **2014**, *4*, 1400739, DOI: 10.1002/aenm.201400739.

(11) Britto, R. J.; Benck, J. D.; Young, J. L.; Hahn, C.; Deutsch, T. G.; Jaramillo, T. F. Molybdenum Disulfide as a Protection Layer and Catalyst for Gallium Indium Phosphide Solar Water Splitting Photocathodes. *J. Phys. Chem. Lett.* **2016**, *7*, 2044–2049, DOI: 10.1021/acs.jpclett.6b00563.

(12) Lancaster, M.; Mow, R.; Liu, J.; Cheek, Q.; Macinnes, M. M.; Al-Jassim, M. M.; Deutsch, T. G.; Young, J. L.; Maldonado, S. Protection of $GaInP_2$ Photocathodes by Direct Photoelectrodeposition of MoS_x Thin Films. *ACS Appl. Mater. Interfaces* **2019**, *11*, 25115–25122, DOI: 10.1021/acsami.9b03742.

(13) Gu, J.; Aguiar, J. A.; Ferrere, S.; Steirer, K. X.; Yan, Y.; Xiao, C.; Young, J. L.; Al-Jassim, M.; Neale, N. R.; Turner, J. A. A Graded Catalytic–Protective Layer for an Efficient and Stable Water-Splitting Photocathode. *Nat. Energy* **2017**, *2*, 16192, DOI: 10.1038/nenergy.2016.192.

(14) Lim, H.; Young, J. L.; Geisz, J. F.; Friedman, D. J.; Deutsch, T. G.; Yoon, J. High Performance III-V Photoelectrodes for Solar Water Splitting via Synergistically Tailored Structure and Stoichiometry. *Nat. Commun.* **2019**, *10*, 3388, DOI: 10.1038/s41467-019-11351-1.

(15) Laursen, A. B.; Pedersen, T.; Malacrida, P.; Seger, B.; Hansen, O.; Vesborg, P. C. K.; Chorkendorff, I. MoS_2 - An Integrated Protective and Active Layer on n^+p-Si for Solar H_2 Evolution. *Phys. Chem. Chem. Phys.* **2013**, *15*, 20000–20004, DOI: 10.1039/c3cp52890a.

(16) Young, J. L.; Steiner, M. A.; Döscher, H.; France, R. M.; Turner, J. A.; Deutsch, T. G. Direct Solar-to-Hydrogen Conversion via Inverted Metamorphic Multi-Junction Semiconductor Architectures. *Nat. Energy* **2017**, *2*, 17028, DOI: 10.1038/nenergy.2017.28.

(17) Jain, N.; Geisz, J. F.; France, R. M.; Norman, A. G.; Steiner, M. A. Enhanced Current Collection in 1.7 EV GaInAsP Solar Cells Grown on GaAs by Metalorganic Vapor Phase Epitaxy. *IEEE J. Photovoltaics* **2017**, *7*, 927–933, DOI: 10.1109/JPHOTOV.2017.2655035.

(18) Jain, N.; Schulte, K. L.; Geisz, J. F.; Friedman, D. J.; France, R. M.; Perl, E. E.; Norman, A. G.; Guthrey, H. L.; Steiner, M. A. High-Efficiency Inverted Metamorphic 1.7/1.1 EV GaInAsP/GaInAs Dual-Junction Solar Cells. *Appl. Phys. Lett.* **2018**, *112*, 053905, DOI: 10.1063/1.5008517.

(19) Seitz, L. C.; Chen, Z.; Forman, A. J.; Pinaud, B. A.; Benck, J. D.; Jaramillo, T. F. Modeling Practical Performance Limits of Photoelectrochemical Water Splitting Based on the Current State of Materials Research. *ChemSusChem* **2014**, *7*, 1372–1385, DOI: 10.1002/cssc.201301030.

(20) Geisz, J. F.; Levander, A. X.; Norman, A. G.; Jones, K. M.; Romero, M. J. *In Situ* Stress Measurement for MOVPE Growth of High Efficiency Lattice-Mismatched Solar Cells. *J. Cryst. Growth* **2008**, *310*, 2339–2344, DOI: 10.1016/j.jcrysgro.2007.11.048.

(21) Steiner, M. A.; Barraugh, C. D.; Aldridge, C. W.; Alvarez, I. B.; Friedman, D. J.; Ekins-Daukes, N. J.; Deutsch, T. G.; Young, J. L. Photoelectrochemical Water Splitting Using Strain-Balanced Multiple Quantum Well Photovoltaic Cells. *Sustain. Energy Fuels* **2019**, *3*, 2837–2844, DOI: 10.1039/c9se00276f.

(22) Young, J. L.; Steirer, K. X.; Dzara, M. J.; Turner, J. A.; Deutsch, T. G. Remarkable Stability of Unmodified GaAs Photocathodes during Hydrogen Evolution in Acidic Electrolyte. *J. Mater. Chem. A* **2016**, *4*, 2831–2836, DOI: 10.1039/C5TA07648J.

(23) Deutsch, T. G.; Koval, C. A.; Turner, J. A. III−V Nitride Epilayers for Photoelectrochemical Water Splitting: GaPN and GaAsPN. *J. Phys. Chem. B* **2006**, *110*, 25297–25307, DOI: 10.1021/jp0652805.

(24) ASTM International. *ASTM G173-03(2012) Standard Tables for Reference Solar Spectral Irradiances: Direct Normal and Hemispherical on 37° Tilted Surface*; West Conshohocken, PA, 2012.

(25) Döscher, H.; Young, J. L.; Geisz, J. F.; Turner, J. A.; Deutsch, T. G. Solar-to-Hydrogen Efficiency: Shining Light on Photoelectrochemical Device Performance. *Energy Environ. Sci.* **2016**, *9*, 74–80, DOI: 10.1039/C5EE03206G.

(26) McCrory, C. C. L.; Jung, S.; Ferrer, I. M.; Chatman, S. M.; Peters, J. C.; Jaramillo, T. F. Benchmarking Hydrogen Evolving Reaction and Oxygen Evolving Reaction Electrocatalysts for Solar Water Splitting Devices. *J. Am. Chem. Soc.* **2015**, *137*, 4347–4357, DOI: 10.1021/ja510442p.

(27) McCrory, C. C. L.; Jung, S.; Peters, J. C.; Jaramillo, T. F. Benchmarking Heterogeneous Electrocatalysts for the Oxygen Evolution Reaction. *J. Am. Chem. Soc.* **2013**, *135*, 16977–16987, DOI: 10.1021/ja407115p.

(28) Yang, Y.; Gu, J.; Young, J. L.; Miller, E. M.; Turner, J. A.; Neale, N. R.; Beard, M. C. Semiconductor Interfacial Carrier Dynamics via Photoinduced Electric Fields. *Science* **2015**, *350*, 1061–1065, DOI: 10.1126/science.aad3459.

(29) Chen, Z.; Jaramillo, T. F.; Deutsch, T. G.; Kleiman-Shwarsctein, A.; Forman, A. J.; Gaillard, N.; Garland, R.; Takanabe, K.; Heske, C.; Sunkara, M.; McFarland, E. W.; Domen, K.;

Milled, E. L.; Dinh, H. N. Accelerating Materials Development for Photoelectrochemical Hydrogen Production: Standards for Methods, Definitions, and Reporting Protocols. *J. Mater. Res.* **2010**, *25*, 3–16, DOI: 10.1557/jmr.2010.0020.

(30) Haussener, S.; Hu, S.; Xiang, C.; Weber, A. Z.; Lewis, N. S. Simulations of the Irradiation and Temperature Dependence of the Efficiency of Tandem Photoelectrochemical Water-Splitting Systems. *Energy Environ. Sci.* **2013**, *6*, 3605–3618, DOI: 10.1039/c3ee41302k.

(31) Welter, K.; Smirnov, V.; Becker, J. P.; Borowski, P.; Hoch, S.; Maljusch, A.; Jaegermann, W.; Finger, F. The Influence of Operation Temperature and Variations of the Illumination on the Performance of Integrated Photoelectrochemical Water-Splitting Devices. *ChemElectroChem* **2017**, *4*, 2099–2108, DOI: 10.1002/celc.201700112.

(32) Moon, R. L.; Antypas, G. A.; James, L. W. Bandgap and Lattice Constant of GaInAsP as a Function of Alloy Composition. *J. Electron. Mater.* **1974**, *3*, 635–644, DOI: 10.1007/BF02655291.

(33) Khaselev, O.; Turner, J. A. Electrochemical Stability of P-$GaInP_2$ in Aqueous Electrolytes Toward Photoelectrochemical Water Splitting. *J. Electrochem. Soc.* **1998**, *145*, 3335–3339, DOI: 10.1149/1.1838808.

(34) Walter, M. G.; Warren, E. L.; McKone, J. R.; Boettcher, S. W.; Mi, Q.; Santori, E. A.; Lewis, N. S. Solar Water Splitting Cells. *Chem. Rev.* **2010**, *110*, 6446–6473, DOI: 10.1021/cr1002326.

(35) Chen, Z.; Cummins, D.; Reinecke, B. N.; Clark, E.; Sunkara, M. K.; Jaramillo, T. F. Core-Shell MoO_3-MoS_2 Nanowires for Hydrogen Evolution: A Functional Design for Electrocatalytic Materials. *Nano Lett.* **2011**, *11*, 4168–4175, DOI: 10.1021/nl2020476.

(36) Li, L.; Yang, J.; Ali-Löytty, H.; Weng, T. C.; Toma, F. M.; Sokaras, D.; Sharp, I. D.; Nilsson, A. Operando Observation of Chemical Transformations of Iridium Oxide during Photoelectrochemical Water Oxidation. *ACS Appl. Energy Mater.* **2019**, *2*, 1371–1379, DOI: 10.1021/acsaem.8b01945.

(37) Fracchia, M.; Cristino, V.; Vertova, A.; Rondinini, S.; Caramori, S.; Ghigna, P.; Minguzzi, A. Operando X-Ray Absorption Spectroscopy of WO3 Photoanodes. *Electrochim. Acta* **2019**, *320*, 134561, DOI: 10.1016/j.electacta.2019.134561.

(38) Conzuelo, F.; Sliozberg, K.; Gutkowski, R.; Grutzke, S.; Nebe, M.; Schuhmann, W. High-Resolution Analysis of Photoanodes for Water Splitting by Means of Scanning Photoelectrochemical Microscopy. *Anal. Chem.* **2017**, *89*, 1222–1228, DOI: 10.1021/acs.analchem.6b03706.

(39) Bae, J. H.; Nepomnyashchii, A. B.; Wang, X.; Potapenko, D. V.; Mirkin, M. V. Photo-Scanning Electrochemical Microscopy on the Nanoscale with Through-Tip Illumination. *Anal. Chem.* **2019**, *91*, 12601–12605, DOI: 10.1021/acs.analchem.9b03347.

(40) Schermer, J. J.; Mulder, P.; Bauhuis, G. J.; Voncken, M. M. A. J.; van Deelen, J.; Haverkamp, E.; Larsen, P. K. Epitaxial Lift-Off for Large Area Thin Film III/V Devices. *Phys. Status Solidi A* **2005**, *202*, 501–508, DOI: 10.1002/pssa.200460410.

(41) Shahrjerdi, D.; Bedell, S. W.; Ebert, C.; Bayram, C.; Hekmatshoar, B.; Fogel, K.; Lauro, P.; Gaynes, M.; Gokmen, T.; Ott, J. A.; Sadana, D. K. High-Efficiency Thin-Film InGaP/InGaAs/Ge Tandem Solar Cells Enabled by Controlled Spalling Technology. *Appl. Phys. Lett.* **2012**, *100*, 12–15, DOI: 10.1063/1.3681397.

(42) Simon, J.; Schulte, K. L.; Young, D. L.; Haegel, N. M.; Ptak, A. J. GaAs Solar Cells Grown by Hydride Vapor-Phase Epitaxy and the Development of GaInP Cladding Layers. *IEEE J. Photovoltaics* **2016**, *6*, 191–195, DOI: 10.1109/JPHOTOV.2015.2501723.

(43) Woodhouse, M.; Goodrich, A. A. *Manufacturing Cost Analysis Relevant to Single- and Dual-Junction Photovoltaic Cells Fabricated with III-Vs and III-Vs Grown on Czochralski Silicon*; Golden, CO, 2013.

(44) Nielander, A. C.; Shaner, M. R.; Papadantonakis, K. M.; Francis, S. A.; Lewis, N. S. A Taxonomy for Solar Fuels Generators. *Energy Environ. Sci.* **2015**, *8*, 16–25, DOI: 10.1039/c4ee02251c.

(45) Khaselev, O.; Turner, J. A. A Monolithic Photovoltaic-Photoelectrochemical Device for Hydrogen Production via Water Splitting. *Science* **1998**, *280*, 425–427, DOI: 10.1126/science.280.5362.425.

(46) Verlage, E.; Hu, S.; Liu, R.; Jones, R. J. R.; Sun, K.; Xiang, C.; Lewis, N. S.; Atwater, H. A. A Monolithically Integrated, Intrinsically Safe, 10% Efficient, Solar-Driven Water-Splitting System Based on Active, Stable Earth-Abundant Electrocatalysts in Conjunction with Tandem III–V Light Absorbers Protected by Amorphous TiO2 Films. *Energy Environ. Sci.* **2015**, *8*, 3166–3172, DOI: 10.1039/C5EE01786F.

(47) Wang, Y.; Schwartz, J.; Gim, J.; Hovden, R.; Mi, Z. Stable Unassisted Solar Water Splitting on Semiconductor Photocathodes Protected by Multifunctional GaN Nanostructures. *ACS Energy Lett.* **2019**, *4*, 1541–1548, DOI: 10.1021/acsenergylett.9b00549.

(48) Pan, L.; Kim, J. H.; Mayer, M. T.; Son, M. K.; Ummadisingu, A.; Lee, J. S.; Hagfeldt, A.; Luo, J.; Grätzel, M. Boosting the Performance of Cu_2O Photocathodes for Unassisted Solar Water Splitting Devices. *Nat. Catal.* **2018**, *1*, 412–420, DOI: 10.1038/s41929-018-0077-6.

(49) Lin, G. H.; Kapur, M.; Kainthla, R. C.; Bockris, J. O. M. One Step Method to Produce Hydrogen by a Triple Stack Amorphous Silicon Solar Cell. *Appl. Phys. Lett.* **1989**, *55*, 386–387, DOI: 10.1063/1.101879.

(50) Wang, Y.; Wu, Y.; Schwartz, J.; Sung, S. H.; Hovden, R.; Mi, Z. A Single-Junction Cathodic Approach for Stable Unassisted Solar Water Splitting. *Joule* **2019**, *3*, 2444–2456, DOI: 10.1016/j.joule.2019.07.022.

(51) Kainthla, R. C.; Zelenay, B.; Bockris, J. O. Significant Efficiency Increase in Self-Driven Photoelectrochemical Cell for Water Photoelectrolysis. *J. Electrochem. Soc.* **1987**, *134*, 841–845, DOI: 10.1149/1.2100583.

(52) Higashi, T.; Kaneko, H.; Minegishi, T.; Kobayashi, H.; Zhong, M.; Kuang, Y.; Hisatomi, T.; Katayama, M.; Takata, T.; Nishiyama, H.; Yamada, T.; Domen, K. Overall Water Splitting by Photoelectrochemical Cells Consisting of $(ZnSe)_{0.85}(CuIn_{0.7}Ga_{0.3}Se_2)_{0.15}$ Photocathodes and $BiVO_4$ Photoanodes. *Chem. Commun.* **2017**, *53*, 11674–11677, DOI: 10.1039/c7cc06637f.

(53) Reece, S. Y.; Hamel, J. A.; Sung, K.; Jarvi, T. D.; Esswein, A. J.; Pijpers, J. J. H.; Nocera, D. G. Wireless Solar Water Splitting Using Silicon-Based Semiconductors and Earth-Abundant Catalysts. *Science* **2011**, *334*, 645–648, DOI: 10.1126/science.1209816.

(54) Huang, D.; Wang, K.; Yu, L.; Nguyen, T. H.; Ikeda, S.; Jiang, F. Over 1% Efficient Unbiased Stable Solar Water Splitting Based on a Sprayed Cu_2ZnSnS_4 Photocathode Protected by a HfO_2 Photocorrosion-Resistant Film. *ACS Energy Lett.* **2018**, *3*, 1875–1881, DOI: 10.1021/acsenergylett.8b01005.

(55) Varadhan, P.; Fu, H.-C.; Kao, Y.-C.; Horng, R.-H.; He, J.-H. An Efficient and Stable Photoelectrochemical System with 9% Solar-to-Hydrogen Conversion Efficiency via InGaP/GaAs Double Junction. *Nat. Commun.* **2019**, *10*, 5282, DOI: 10.1038/s41467-019-12977-x.

(56) Fan, R.; Cheng, S.; Huang, G.; Wang, Y.; Zhang, Y.; Vanka, S.; Botton, G. A.; Mi, Z.; Shen, M. Unassisted Solar Water Splitting with 9.8% Efficiency and over 100 h Stability Based on Si Solar Cells and Photoelectrodes Catalyzed by Bifunctional Ni-Mo/Ni. *J. Mater. Chem. A* **2019**, *7*, 2200–2209, DOI: 10.1039/c8ta10165e.

(57) Shi, X.; Jeong, H.; Oh, S. J.; Ma, M.; Zhang, K.; Kwon, J.; Choi, I. T.; Choi, I. Y.; Kim, H. K.; Kim, J. K.; Park, J. H. Unassisted Photoelectrochemical Water Splitting Exceeding 7% Solar-to-Hydrogen Conversion Efficiency Using Photon Recycling. *Nat. Commun.* **2016**, *7*, DOI: 10.1038/ncomms11943.

(58) Shi, X.; Zhang, K.; Shin, K.; Ma, M.; Kwon, J.; Choi, I. T.; Kim, J. K.; Kim, H. K.; Wang, D. H.; Park, J. H. Unassisted Photoelectrochemical Water Splitting beyond 5.7% Solar-to-Hydrogen Conversion Efficiency by a Wireless Monolithic Photoanode/Dye-Sensitised Solar Cell Tandem Device. *Nano Energy* **2015**, *13*, 182–191, DOI: 10.1016/j.nanoen.2015.02.018.

(59) Kim, J. H.; Jo, Y.; Kim, J. H.; Jang, J. W.; Kang, H. J.; Lee, Y. H.; Kim, D. S.; Jun, Y.; Lee, J. S. Wireless Solar Water Splitting Device with Robust Cobalt-Catalyzed, Dual-Doped $BiVO_4$ Photoanode and Perovskite Solar Cell in Tandem: A Dual Absorber Artificial Leaf. *ACS Nano* **2015**, *9*, 11820–11829, DOI: 10.1021/acsnano.5b03859.

(60) Kim, J. H.; Jang, J. W.; Jo, Y. H.; Abdi, F. F.; Lee, Y. H.; Van De Krol, R.; Lee, J. S. Hetero-Type Dual Photoanodes for Unbiased Solar Water Splitting with Extended Light Harvesting. *Nat. Commun.* **2016**, *7*, 1–9, DOI: 10.1038/ncomms13380.

(61) Zhang, S.; Shen, L.; Ye, T.; Kong, K.; Ye, H.; Ding, H.; Hu, Y.; Hua, J. Noble-Metal-Free Perovskite-$BiVO_4$ Tandem Device with Simple Preparation Method for Unassisted Solar-Water-Splitting. *Energy & Fuels* **2020**, acs.energyfuels.0c00432, DOI: 10.1021/acs.energyfuels.0c00432.

(62) Kim, J. H.; Han, S.; Jo, Y. H.; Bak, Y.; Lee, J. S. A Precious Metal-Free Solar Water Splitting Cell with a Bifunctional Cobalt Phosphide Electrocatalyst and Doubly Promoted Bismuth Vanadate Photoanode. *J. Mater. Chem. A* **2018**, *6*, 1266–1274, DOI: 10.1039/c7ta09134f.

(63) Kosar, S.; Pihosh, Y.; Turkevych, I.; Mawatari, K.; Uemura, J.; Kazoe, Y.; Makita, K.; Sugaya, T.; Matsui, T.; Fujita, D.; Tosa, M.; Struk, Y. M.; Kondo, M.; Kitamori, T. Tandem Photovoltaic–Photoelectrochemical GaAs/InGaAsP–WO_3/$BiVO_4$ Device for Solar Hydrogen Generation. *Jpn. J. Appl. Phys.* **2016**, *55*, 04ES01, DOI: 10.7567/JJAP.55.04ES01.

(64) Gurudayal; Sabba, D.; Kumar, M. H.; Wong, L. H.; Barber, J.; Grätzel, M.; Mathews, N. Perovskite–Hematite Tandem Cells for Efficient Overall Solar Driven Water Splitting. *Nano Lett.* **2015**, *15*, 3833–3839, DOI: 10.1021/acs.nanolett.5b00616.

(65) Dias, P.; Schreier, M.; Tilley, S. D.; Luo, J.; Azevedo, J.; Andrade, L.; Bi, D.; Hagfeldt, A.; Mendes, A.; Grätzel, M.; Mayer, M. T. Transparent Cuprous Oxide Photocathode Enabling a Stacked Tandem Cell for Unbiased Water Splitting. *Adv. Energy Mater.* **2015**, *5*, 1–9, DOI: 10.1002/aenm.201501537.

(66) Gaillard, N.; Chang, Y.; Kaneshiro, J.; Deangelis, A.; Miller, E. L. Status of Research on Tungsten Oxide-Based Photoelectrochemical Devices at the University of Hawai'i. *Sol. Hydrog. Nanotechnol. V* **2010**, *7770*, 77700V, DOI: 10.1117/12.860970.

(67) Brillet, J.; Yum, J. H.; Cornuz, M.; Hisatomi, T.; Solarska, R.; Augustynski, J.; Graetzel, M.; Sivula, K. Highly Efficient Water Splitting by a Dual-Absorber Tandem Cell. *Nat. Photonics* **2012**, *6*, 824–828, DOI: 10.1038/nphoton.2012.265.

(68) Han, L.; Abdi, F. F.; Van De Krol, R.; Liu, R.; Huang, Z.; Lewerenz, H. J.; Dam, B.; Zeman, M.; Smets, A. H. M. Efficient Water-Splitting Device Based on a Bismuth Vanadate Photoanode and Thin-Film Silicon Solar Cells. *ChemSusChem* **2014**, *7*, 2832–2838, DOI: 10.1002/cssc.201402456.

(69) Abdi, F. F.; Han, L.; Smets, A. H. M.; Zeman, M.; Dam, B.; Van De Krol, R. Efficient Solar Water Splitting by Enhanced Charge Separation in a Bismuth Vanadate-Silicon Tandem Photoelectrode. *Nat. Commun.* **2013**, *4*, 2195, DOI: 10.1038/ncomms3195.

(70) Shin, K.; Park, J. H. Highly Transparent Dual-Sensitized Titanium Dioxide Nanotube Arrays for Spontaneous Solar Water Splitting Tandem Configuration. *ACS Appl. Mater. Interfaces* **2015**, *7*, 18429–18434, DOI: 10.1021/acsami.5b04521.

(71) Meng, L.; Wang, M.; Sun, H.; Tian, W.; Xiao, C.; Wu, S.; Cao, F.; Li, L. Designing a Transparent $CdIn_2S_4/In_2S_3$ Bulk-Heterojunction Photoanode Integrated with a Perovskite Solar Cell for Unbiased Water Splitting. *Adv. Mater.* **2020**, 2002893, DOI: 10.1002/adma.202002893.

(72) Ding, C.; Qin, W.; Wang, N.; Liu, G.; Wang, Z.; Yan, P.; Shi, J.; Li, C. Solar-to-Hydrogen Efficiency Exceeding 2.5% Achieved for Overall Water Splitting with an All Earth-Abundant Dual-Photoelectrode. *Phys. Chem. Chem. Phys.* **2014**, *16*, 15608–15614, DOI: 10.1039/c4cp02391a.

(73) Hayashi, T.; Niishiro, R.; Ishihara, H.; Yamaguchi, M.; Jia, Q.; Kuang, Y.; Higashi, T.; Iwase, A.; Minegishi, T.; Yamada, T.; Domen, K.; Kudo, A. Powder-Based $(CuGa_{1-y}In_y)_{1-x}Zn_{2x}S_2$ Solid Solution Photocathodes with a Largely Positive Onset Potential for Solar Water Splitting. *Sustain. Energy Fuels* **2018**, *2*, 2016–2024, DOI: 10.1039/C8SE00079D.

(74) Kobayashi, H.; Sato, N.; Orita, M.; Kuang, Y.; Kaneko, H.; Minegishi, T.; Yamada, T.; Domen, K. Development of Highly Efficient $CuIn_{0.5}Ga_{0.5}Se_2$-Based Photocathode and Application to Overall Solar Driven Water Splitting. *Energy Environ. Sci.* **2018**, *11*, 3003–3009, DOI: 10.1039/c8ee01783b.

(75) May, M. M.; Lewerenz, H. J.; Lackner, D.; Dimroth, F.; Hannappel, T. Efficient Direct Solar-to-Hydrogen Conversion by in Situ Interface Transformation of a Tandem Structure. *Nat. Commun.* **2015**, *6*, 4–10, DOI: 10.1038/ncomms9286.

(76) Chen, M.; Liu, Y.; Li, C.; Li, A.; Chang, X.; Liu, W.; Sun, Y.; Wang, T.; Gong, J. Spatial Control of Cocatalysts and Elimination of Interfacial Defects towards Efficient and Robust CIGS Photocathodes for Solar Water Splitting. *Energy Environ. Sci.* **2018**, *11*, 2025–2034, DOI: 10.1039/c7ee03650g.

(77) Martinez-Garcia, A.; Russell, H. B.; Paxton, W.; Ravipati, S.; Calero-Barney, S.; Menon, M.; Richter, E.; Young, J. L.; Deutsch, T. G.; Sunkara, M. K. Unassisted Water Splitting Using a $GaSb_xP_{(1-x)}$ Photoanode. *Adv. Energy Mater.* **2018**, *8*, 1–9, DOI: 10.1002/aenm.201703247.

(78) Wang, X.; Peng, K. Q.; Hu, Y.; Zhang, F. Q.; Hu, B.; Li, L.; Wang, M.; Meng, X. M.; Lee, S. T. Silicon/Hematite Core/Shell Nanowire Array Decorated with Gold Nanoparticles for Unbiased Solar Water Oxidation. *Nano Lett.* **2014**, *14*, 18–23, DOI: 10.1021/nl402205f.

(79) Kang, D.; Young, J. L.; Lim, H.; Klein, W. E.; Chen, H.; Xi, Y.; Gai, B.; Deutsch, T. G.; Yoon, J. Printed Assemblies of GaAs Photoelectrodes with Decoupled Optical and Reactive Interfaces for Unassisted Solar Water Splitting. *Nat. Energy* **2017**, *2*, 1–9, DOI: 10.1038/nenergy.2017.43.

(80) Sakai, Y.; Sugahara, S.; Matsumura, M.; Nakato, Y.; Tsubomura, H. Photoelectrochemical Water Splitting by Tandem Type and Heterojunction Amorphous Silicon Electrodes. *Can. J. Chem.* **1988**, *66*, 1853–1856, DOI: 10.1139/v88-299.

(81) Peng, Y.; Govindaraju, G. V.; Lee, D. K.; Choi, K. S.; Andrew, T. L. Integrating a Semitransparent, Fullerene-Free Organic Solar Cell in Tandem with a $BiVO_4$ Photoanode for Unassisted Solar Water Splitting. *ACS Appl. Mater. Interfaces* **2017**, *9*, 22449–22455, DOI: 10.1021/acsami.7b04486.

(82) Karuturi, S. K.; Shen, H.; Sharma, A.; Beck, F. J.; Varadhan, P.; Duong, T.; Narangari, P. R.; Zhang, D.; Wan, Y.; He, J.; Tan, H. H.; Jagadish, C.; Catchpole, K. Over 17% Efficiency Stand-Alone Solar Water Splitting Enabled by Perovskite-Silicon Tandem Absorbers. *Adv. Energy Mater.* **2020**, *2000772*, 2000772, DOI: 10.1002/aenm.202000772.

(83) Morales-Guio, C. G.; Mayer, M. T.; Yella, A.; Tilley, S. D.; Grätzel, M.; Hu, X. An Optically Transparent Iron Nickel Oxide Catalyst for Solar Water Splitting. *J. Am. Chem. Soc.* **2015**, *137*, 9927–9936, DOI: 10.1021/jacs.5b05544.

(84) Wang, D.; Hu, J.; Sherman, B. D.; Sheridan, M. V.; Yan, L.; Dares, C. J.; Zhu, Y.; Li, F.; Huang, Q.; You, W.; Meyer, T. J. A Molecular Tandem Cell for Efficient Solar Water Splitting. *Proc. Natl. Acad. Sci.* **2020**, 202001753, DOI: 10.1073/pnas.2001753117.

(85) Park, J. H.; Bard, A. J. Photoelectrochemical Tandem Cell with Bipolar Dye-Sensitized Electrodes for Vectorial Electron Transfer for Water Splitting. *Electrochem. Solid-State Lett.* **2006**, *9*, 6–9, DOI: 10.1149/1.2140497.

(86) Baek, J. H.; Kim, B. J.; Han, G. S.; Hwang, S. W.; Kim, D. R.; Cho, I. S.; Jung, H. S. $BiVO_4/WO_3/SnO_2$ Double-Heterojunction Photoanode with Enhanced Charge Separation and Visible-Transparency for Bias-Free Solar Water-Splitting with a Perovskite Solar Cell. *ACS Appl. Mater. Interfaces* **2017**, *9*, 1479–1487, DOI: 10.1021/acsami.6b12782.

(87) Luo, J.; Li, Z.; Nishiwaki, S.; Schreier, M.; Mayer, M. T.; Cendula, P.; Lee, Y. H.; Fu, K.; Cao, A.; Nazeeruddin, M. K.; Romanyuk, Y. E.; Buecheler, S.; Tilley, S. D.; Wong, L. H.; Tiwari, A. N.; Grätzel, M. Targeting Ideal Dual-Absorber Tandem Water Splitting Using Perovskite Photovoltaics and $CuIn_xGa_{1-x}Se_2$ Photocathodes. *Adv. Energy Mater.* **2015**, *5*, 1–8, DOI: 10.1002/aenm.201501520.

(88) Chen, Y. S.; Manser, J. S.; Kamat, P. V. All Solution-Processed Lead Halide Perovskite-$BiVO_4$ Tandem Assembly for Photolytic Solar Fuels Production. *J. Am. Chem. Soc.* **2015**, *137*, 974–981, DOI: 10.1021/ja511739y.

(89) Gurudayal; John, R. A.; Boix, P. P.; Yi, C.; Shi, C.; Scott, M. C.; Veldhuis, S. A.; Minor, A. M.; Zakeeruddin, S. M.; Wong, L. H.; Grätzel, M.; Mathews, N. Atomically Altered Hematite for Highly Efficient Perovskite Tandem Water-Splitting Devices. *ChemSusChem* **2017**, *10*, 2449–2456, DOI: 10.1002/cssc.201700159.

(90) Tan, C. S. S.; Kemp, K. W.; Braun, M.; Meng, A. C.; Tan, W.; Chidsey, C. E. D.; Ma, W.; Moghadam, F.; Mc Intyre, P. C. >10% Solar-to-Hydrogen Efficiency Unassisted Water Splitting on ALD-Protected Silicon Heterojunction Solar Cells. *Sustain. Energy Fuels* **2019**, *3*, 1490–1500, DOI: 10.1039/c9se00110g.

(91) Brillet, J.; Comuz, M.; Formal, F. Le; Yum, J. H.; Grätzel, M.; Sivula, K. Examining Architectures of Photoanode-Photovoltaic Tandem Cells for Solar Water Splitting. *J. Mater. Res.* **2010**, *25*, 17–24, DOI: 10.1557/jmr.2010.0009.

(92) King, L. A.; Hellstern, T. R.; Park, J.; Sinclair, R.; Jaramillo, T. F. Highly Stable Molybdenum Disulfide Protected Silicon Photocathodes for Photoelectrochemical Water Splitting. *ACS Appl. Mater. Interfaces* **2017**, *9*, 36792–36798, DOI: 10.1021/acsami.7b10749.